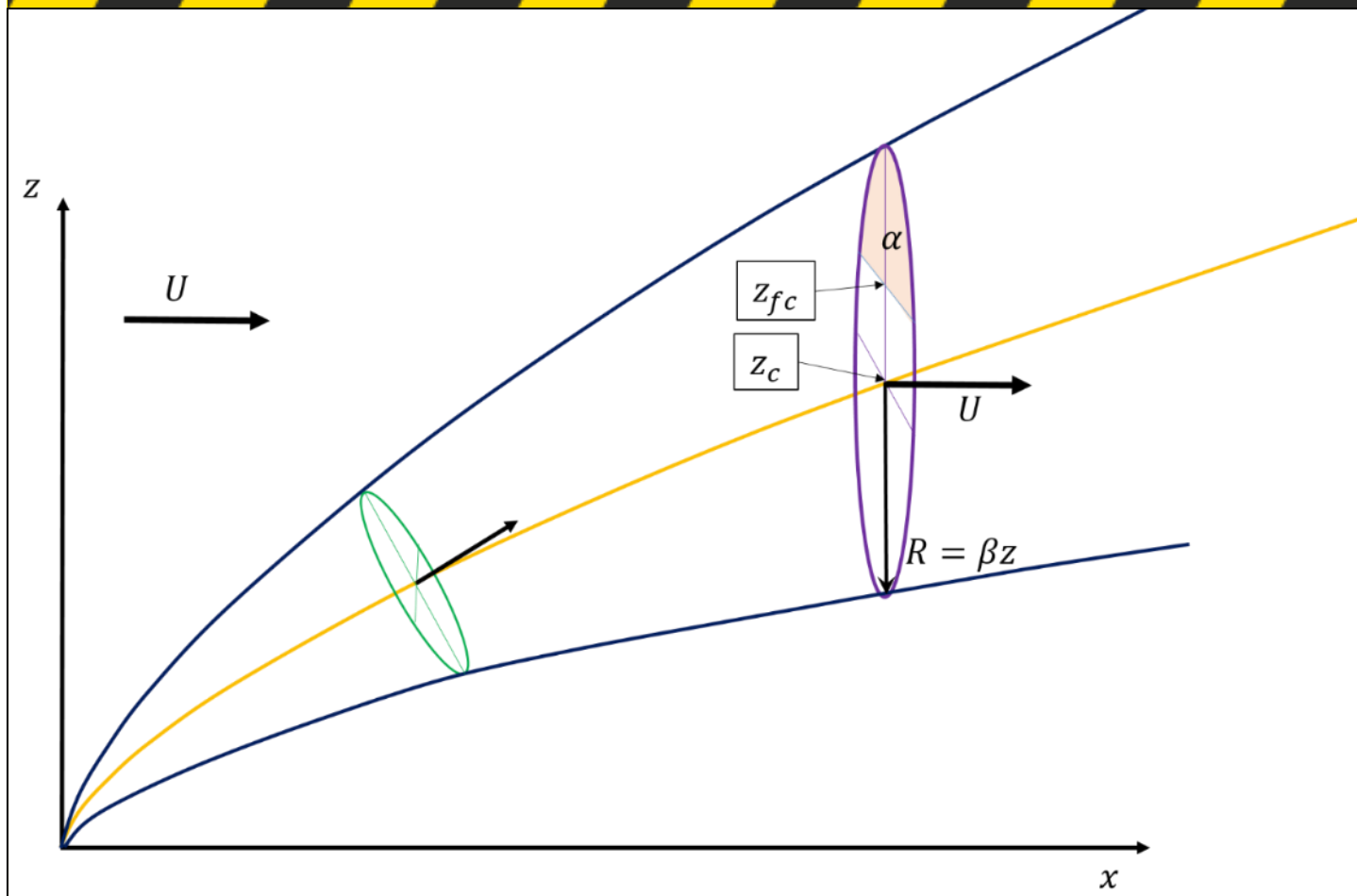


bnhcrc.com.au

MODELS OF BUOYANT PLUME RISE

Kevin Tory
Bureau of Meteorology





Version	Release history	Date
1.0	Initial release of document	18/12/2018



Australian Government
**Department of Industry,
 Innovation and Science**

Business
 Cooperative Research
 Centres Programme

All material in this document, except as identified below, is licensed under the Creative Commons Attribution-Non-Commercial 4.0 International Licence.

- Material not licensed under the Creative Commons licence:
- Department of Industry, Innovation and Science logo
 - Cooperative Research Centres Programme logo
 - Bushfire and Natural Hazards CRC logo
 - Any other logos
 - All photographs, graphics and figures

All content not licenced under the Creative Commons licence is all rights reserved. Permission must be sought from the copyright owner to use this material.



Disclaimer:

The Bureau of Meteorology and the Bushfire and Natural Hazards CRC advise that the information contained in this publication comprises general statements based on scientific research. The reader is advised and needs to be aware that such information may be incomplete or unable to be used in any specific situation. No reliance or actions must therefore be made on that information without seeking prior expert professional, scientific and technical advice. To the extent permitted by law, the Bureau of Meteorology and the Bushfire and Natural Hazards CRC (including its employees and consultants) exclude all liability to any person for any consequences, including but not limited to all losses, damages, costs, expenses and any other compensation, arising directly or indirectly from using this publication (in part or in whole) and any information or material contained in it.

Publisher:

Bushfire and Natural Hazards CRC

December 2018

Citation: Tory, K. (2018) Models of buoyant plume rise. Melbourne: Bushfire and Natural Hazards CRC.



TABLE OF CONTENTS

ACKNOWLEDGMENTS	4
FOREWORD	5
HISTORY	6
Motivation	6
Issues	6
METHOD	8
Plume-rise equations	8
Solutions	9
Morton-Taylor-Turner upright plume analytic solutions	10
Briggs bent-over plume analytic Solutions	10
Numerical Solutions	12
Tohidi and kaye plume equations	13
In-plume time and space varying distributions	13
WILDFIRE APPLICATIONS	16
History	16
Recent interest	16
Adressing the three general concerns	19
SUMMARY AND DISCUSSION	23
REFERENCES	24



ACKNOWLEDGMENTS

Thanks to Jeff Kepert, Serena Schroeter, Andrew Dowdy and Alan Wain for reviewing the document.



FOREWORD

This document has been written to provide a review of the plume-rise literature that is of relevance to two sub-projects of the "Improved prediction of severe weather to reduce community impact" project funded by the Bushfire and Natural Hazards Cooperative Research Centre (BNHCRC). The plume rise literature is a vast body of work that has been reviewed several times by leading experts (e.g., Scorer 1959, Briggs 1975, Briggs 1984, Weil 1988, Arya 1999 Chapter 10). This document borrows from the review papers and targets only background information relevant to the above-mentioned sub-projects: an ember transport model, and a pyrocumulonimbus (pyroCb) prediction tool.

The ember transport model is being designed as a parameterization tool that represents the distribution of burning embers carried by a wildfire plume. It is computationally very cheap to run and can be used off-line or within existing fire-spread or coupled fire-atmosphere models. The model inputs are fire size and intensity, and atmospheric variables such as the background wind field and static stability profile. The plume rise equations are used to determine ember lofting heights and downwind transport.

The pyroCb prediction tool is designed to identify the potential for pyroCb formation from a single atmospheric sounding. It can be applied to observed soundings to give single value estimates and applied to model data (numerical weather prediction models, reanalysis data sets, climate model data) to generate maps of pyroCb threat. A theoretical minimum plume height and buoyancy can be determined from an atmospheric sounding (Tory et al. 2018), which is input to plume rise equations to determine a theoretical minimum fire power required to generate a plume with these minimum qualities.



HISTORY

MOTIVATION

Plume rise studies were born out of the need to design chimney stacks capable of dispersing smoke and other pollutants sufficiently to address local air pollution concerns. It had long been known that under certain atmospheric conditions, ground-level concentrations of pollutants downwind of a chimney decrease with the square of the chimney or "stack" height (e.g., Bosenquet and Pearson (1936, as cited in Briggs 1969). It was later observed that for buoyant plumes and plumes emitted with initial vertical momentum, this inverse square relationship should be extended to the plume centre-line height, the "effective stack height" (e.g., Briggs 1969, Carson and Moses, 1969). Thus, the prediction of plume-rise height became critical for effective chimney design, and plume-rise models began to be developed to optimise chimney height, diameter, effluent ejection speed and buoyancy, based on a range of expected environmental conditions (e.g., wind speed, stratification and turbulence).


ISSUES

Early plume-rise models (dating back to the early 1950's), used empirical relationships between chimney and environmental parameters (Holland 1953), or dimensional analysis techniques to predict maximum plume height (e.g., Scorer 1959). These equations tend to be limited to the parameter space they are tested in and were frequently found to perform poorly. These failures led to an abundance of new and supposedly improved formulae throughout the 1960's (Carson and Moses 1969), but there was a worrying lack of agreement between all the formulae. A quote from the introduction of Briggs 1975 sums up his frustration with the problem:

Techniques for doing this [calculating maximum plume rise] have been developed by at least 50 different people and organisations, probably more than 100 (I gave up counting six years ago). The problem is, they don't all agree. Hardly any of them agree, either with each other or with new observations if they go outside the range of variables of the observations the techniques were originally made to fit.

He goes on to say that much of the confusion is due to inconsistency in definitions, and an inability to observe the actual maximum plume rise. Indeed, the maximum plume rise was often declared before the plume had levelled-off.

While this demonstrates a significant scientific problem, it is nothing compared to the confusion faced by engineers faced with the task of designing chimney stacks to avoid poor surface air quality. Briggs and others appear to be berating the scientific community on their inability to provide a practical solution for engineers to employ. Briggs (1975) noted that different formulae predicted plume rises "ranging over a factor of 10 or more!" and were expressed as functions of a variety of different source parameters and complex meteorological conditions. For example, in 15 different plume rise formulas, wind speed was raised with exponents ranging from -0.33 to -3, and the plume heat term was raised to powers between 0.25 to 1.0 (Carson and Moses 1969). None



of the proposed formulae could be expected to apply in all conditions. The engineers' lot, summarised by Briggs, is "a sad situation indeed".

Briggs recognised the need to express the plume-rise height as a function of downwind distance, as a way to address the issue of unobservable maximum plume-rise. He also recognised that the empirical approach had failed, and that it was past time to return to "the old physics" of "turbulent fluid mechanics". This approach, described below, enabled significant advances in plume-rise understanding (plume rise trajectory prior to final rise, and for final rise in stable conditions), but unresolved issues remained at least until the mid- to late-'80s, when the Briggs (1984) and Weil (1988) review papers were written. Unresolved issues included: partial penetration of stable layers above a buoyant source; the problem of final rise when terminated by ambient turbulence (which has many theoretical solutions, but insufficient data to test them); and plume rise in convective conditions (e.g., generated by surface solar radiative heating, typically during the day when winds are less than about 7 m/s).

Briggs' solutions enabled improved formulae of final-plume-rise heights that are still used today in atmospheric dispersion models. In atmospheric dispersion models, the plume geometry is unimportant, especially if it is contained in only one grid box. Instead, it is the height at which the plume disperses that is required by the model. One example is the Hybrid Single Particle Lagrangian Integrated Trajectory (HySPLIT, e.g., Stein et al. 2015) model, which uses Briggs solutions with modifications suggested by Arya (1999, Eq. 10.15 and the buoyancy dominated plume equations in Table 10.1). Numerous other air quality models that use the Briggs final-plume-rise height equations are listed in the introduction of Gordon et al. (2017) including, GEM-MACH (Im et al. 2015), CMAQ (Byun and Ching 1999) CAMx (Emery et al. 2010) and three models summarised by Holmes (2006): AEROPOL, SCREEN3 and CALGRID¹.

The focus on plume rise in the field of downstream pollutant exposure led to a split in plume studies, with two distinct goals: understanding plume *trajectories*, and understanding plume *material dispersion* (e.g., Zhang and Ghoniem 1993). The Briggs and Weil review papers (each with plume-rise as the key word in the title) concentrate on the former goal. For the wildfire-plume applications we are developing, some representation of the in-plume variability of vertical velocity and buoyancy is essential, which requires consideration of the latter goal also.

¹ While the take-home message of Gordon et al. (2017) is that the Briggs final-plume-rise height equations generally under-estimate recent measurements, these equations are not used in our projects. (Our projects use equations that describe the plume geometry.) Additionally, the Gordon et al. paper is currently in the discussion phase (open to public review prior to final publication), and criticisms have been raised suggesting the discrepancies are due to the complex orography of the observation site, rather than a failure of the Briggs equations (e.g., De Visscher 2018).



METHOD

PLUME-RISE EQUATIONS

The derivation of the integral model begins with equations for the conservation of mass, buoyancy and momentum. Plumes are assumed to have a continuous source and to be continuous along their axes. The physical state of the plume is described "in bulk" by integrating the conservation equations over the area of a plane intersecting the plume at some point along the axis. The "bulk" quantities represent cross-plume mean values, the so-called top-hat profile. The resulting equations describe the rate of change of fluxes of mass, buoyancy and momentum along the plume axis.

More realistic cross-plume distributions of plume quantities can be incorporated. For upright plumes, a Gaussian distribution representing the time-mean flow is very accurate (e.g., Hübner, 2004), whereas the counter-rotating gyres that develop in a bent-over plume are more elliptical in shape than circular (with larger horizontal than vertical extent, e.g., Bennet et al. 1992). This is discussed further below.

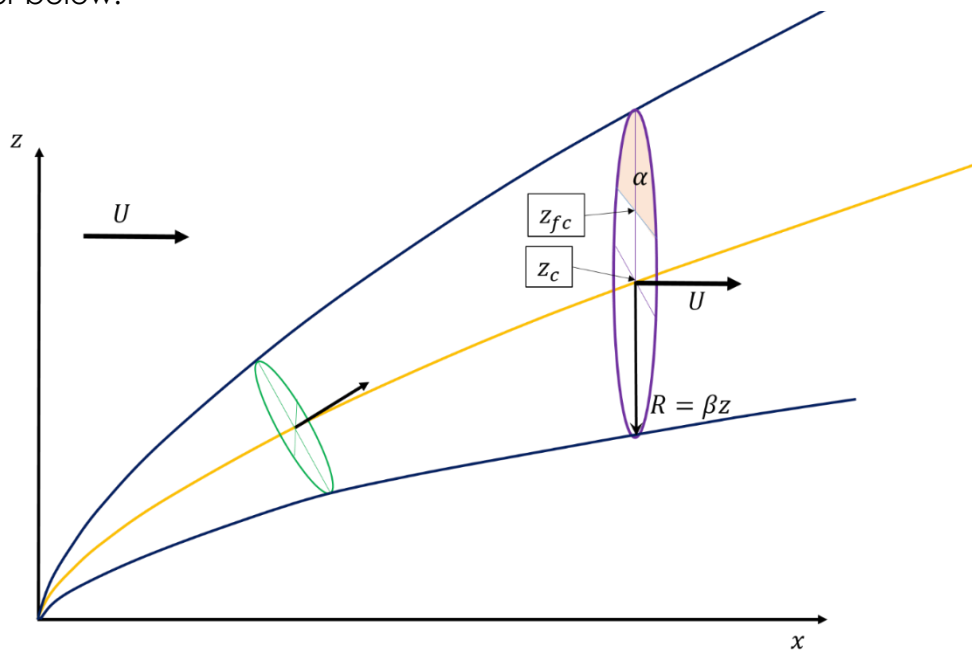


Figure 1: Schematic representation of the plume geometry with the plume centre-line marked in yellow and the plume edges in dark blue. In general solutions are sought to the rate of change of plume flux quantities with distance along the plume centre-line through a circular plume cross-section perpendicular to the plume axis (green circle). The plume is bent-over by the background wind U , which can vary with height. The Briggs simplified geometry considers fluxes through vertical circular plume cross-sections (purple circle), transported by a representative background wind that is assumed to be constant with height. The radius increases linearly with height governed by the constant entrainment parameter β . The shaded area labelled α is used in the pyroCb prediction tool. It represents the fraction of the plume area that must rise above the free convection height, z_{fc} , before deep, moist free-convection can develop. z_c is the plume centre-line height at this downstream position.



Assuming the cross-sectional plane perpendicular to the plume axis is circular (green circle in Fig. 1), and the fluid is Boussinesq (volume is conserved), these equations can be expressed (e.g., Weil 1988) as,

$$\frac{dV}{ds} = \frac{d}{ds} (U_s R^2) = 2RU_n, \quad 1.$$

$$\frac{dm_h}{ds} = \frac{d}{ds} (U_s R^2 u) = -R^2 w \frac{dU}{dz}, \quad 2.$$

$$\frac{dm_v}{ds} = \frac{d}{ds} (U_s R^2 w) = R^2 b, \quad 3.$$

$$\frac{dB}{ds} = \frac{d}{ds} (U_s R^2 b) = N^2 w R^2. \quad 4.$$

Here, U_s , R and U_n are the mean plume flow speed, the cross-sectional radius, and the entrainment velocity respectively. u and w are the mean horizontal and vertical components of the mean plume velocity relative to the background wind (U), N is the Brunt-Väisälä frequency, b is the mean plume buoyancy, and s is the distance along the plume centre-line (e.g., yellow line in Fig. 1). The volume flux (V_{flux}) is the product of U_s and the plume cross-sectional area,

$$V_{flux} = U_s \pi R^2 = \pi V. \quad 5.$$

The buoyancy flux is the product of the volume flux and b ,

$$B_{flux} = \pi V b = \pi B. \quad 6.$$

Similarly, the horizontal and vertical momentum fluxes are,

$$m_{h,flux} = \pi V u = \pi m_h, \quad 7.$$

$$m_{v,flux} = \pi V w = \pi m_v. \quad 8.$$

The mass flux is the product of the density (ρ) and volume flux,

$$M_{flux} = \rho U_s \pi R^2 = \pi \rho V = \pi M. \quad 9.$$

The heat flux can be expressed as,

$$H_{flux} = C_{pd} \Delta \theta M_{flux} = \frac{\rho C_{pd} \theta_a}{g} B_{flux}, \quad 10.$$

using,

$$b = g \frac{\Delta \theta}{\theta_a}. \quad 11.$$

Here $\Delta \theta = \theta_{pl} - \theta_a$ is the difference between the mean plume potential temperature (θ_{pl}) and the ambient potential temperature θ_a .

SOLUTIONS

For some time after this method was first considered (e.g., Morton et al. 1956), numerical solutions were not possible due to insufficient computing power. The earliest study we could find that solved for a similar set of equations numerically dates to the late 1960's (Hoult et al. 1969), which would have been a very computationally expensive endeavour at the time. Today numerical solutions can be found in fractions of a second on modern computers. The use of analytic solutions continues to this day and remains very valuable for understanding fundamental plume dynamics.

Additional simplifications and assumptions are required to find useful analytic solutions. We argue below that highly simplified analytic solutions are surprisingly good for specific scenarios, and continue to be useful for testing solutions, and for understanding basic plume dynamics (e.g., Tory et al. 2018b).



Perhaps the most important assumption, necessary for both the numerical and analytic solutions, is the closure assumption (i.e., that there is one more independent variable than there are equations). The most common closure assumption, applied to the mass flux equation (Eq. 1), was first proposed by G. I. Taylor (Taylor 1945). It governs the entrainment of mass into the plume, expressing it as an inward velocity U_n applied to the outer plume boundary, termed the entrainment velocity. The entrainment velocity was represented as a linear function of the mean vertical plume velocity, because it was assumed that turbulence in the plume was generated by the shear between the plume and ambient fluid,

$$U_n = \alpha w. \tag{12}$$

This method has been and still is widely used for plumes in environments with small ambient turbulence. Large ambient turbulence requires additional considerations (discussed further below).

MORTON-TAYLOR-TURNER UPRIGHT PLUME ANALYTIC SOLUTIONS

The upright plume solutions of Morton et al. (1956, these solutions are often labelled the MTT solutions after the three authors: Morton, Taylor and Turner) are relatively simple to derive and won't be discussed in any detail here, due to their limited real-world applicability for wildfire applications. Of importance is the difference in entrainment parameter between the MTT upright plume, α , and the bent-over plume entrainment parameter, β . β is much larger than α ($\beta \sim 5\alpha$) because the axis of a bent-over plume is perpendicular to, rather than parallel to, its rise, resulting in more efficient mixing with the ambient fluid (Briggs 1984).

It's worth noting that the Briggs solutions (introduced next) have remarkable similarities to the MTT solutions. (See page 76 of Briggs (1975) for a parallel derivation of the two sets of equations.)

BRIGGS BENT-OVER PLUME ANALYTIC SOLUTIONS

Briggs found analytic solutions to Eqs 1—4 after introducing several simplifications and assumptions. In addition to the simplifications described above (solving for a single mean value per position along the plume axis; the so-called top-hat profile, Boussinesq fluid, and linear relationship between the entrainment velocity and plume vertical velocity), the main assumptions are that the plume cross-sectional geometry is a vertical circle (purple circle in Fig. 1), the background cross-flow wind is constant (U), the background static stability is neutral ($N^2 = 0$) and that the plume horizontal velocity (u , i.e., the velocity in excess of the background wind) is much less than U and can be ignored. This last assumption eliminates the horizontal momentum equation (Eq. 2).

The vertical cross-section geometry allows the remaining differential equations to be expressed with respect to the rate of change of fluxes with downstream distance, x ,

$$\frac{dV}{dx} = \frac{d}{dx} (UR^2) = 2R\beta w, \tag{13}$$

$$\frac{dm_v}{dx} = \frac{d}{dx} (UR^2 w) = R^2 b = B/U, \tag{14}$$



$$\frac{dB}{dx} = \frac{d}{dx}(UR^2b) = 0. \quad 15.$$

From Eq. 15, we can see that UR^2b is constant, which is set to B , and thus the RHS of Eq. 14 reduces to B/U . On the RHS of Eq. 13 we have included Briggs' entrainment parameter β . Briggs expressed Eqs 13 and 14 as vertical derivatives, by multiplying both sides of the equations by U/w , using the relationships $U = dx/dt$ and $w = dz/dt$,

$$\frac{dV}{dz} = \frac{d}{dz}(UR^2) = 2R\beta U, \quad 16.$$

$$\frac{dm_v}{dz} = \frac{d}{dz}(UR^2w) = B/w. \quad 17.$$

The solution to Eq. 16 is trivial yielding $dR/dz = \beta$, and $R = \beta z$, since the integration constant is zero for a point source plume.

Briggs' (1984) derivation of the vertical momentum flux equation (Eq. 17), shows that the buoyancy forcing term on the RHS, acts not only on the fluid inside the plume (the internal plume) but also the mass of ambient air displaced by the plume. This internal plume *plus* displaced ambient air is termed the dynamic plume. Both the internal and dynamic plumes are considered to be circular in vertical cross section, with radii R' and R , and entrainment parameters $\beta' = 0.4$ and $\beta = 0.6$ respectively (Briggs 1984, terminology). These entrainment parameters have been extensively tested against a substantial number of observational data sets and are almost universally accepted. Thus, we essentially have two volume flux equations, with two solutions that apply to different aspects of the plume.

Not surprisingly, the distribution of buoyancy flux (and any smoke particles or chemicals emitted by the fire) is contained within the internal plume, and thus Eq. 15 yields,

$$B = U(\beta'z)^2b. \quad 18.$$

Solutions to the vertical momentum flux equation (Eq. 17) give the famous Briggs plume-rise equation that describes the plume centre-line height z with distance x downstream,

$$z = \left[\left(\frac{3}{2\beta^2} \right) \frac{B_{flux}}{\pi U^3} \right]^{\frac{1}{3}} x^{\frac{2}{3}}. \quad 19.$$

Here B_{flux} (Eq. 6) is proportional to the total heat flux H_{flux} (Eq. 10), which is often termed the "power of the fire" or "fire-power". Plume centre-line examples are illustrated in Fig. 2. The magnitude of the square bracketed term in Eq. 19 determines the relative slope of the curve. The equation shows that for a particular fire-power and entrainment rate the plume becomes increasingly bent-over for increasing wind speeds (e.g., red to blue curves in Fig. 3). Similarly, for a specific wind speed and entrainment rate, the plume becomes increasingly bent-over for decreasing fire-power.

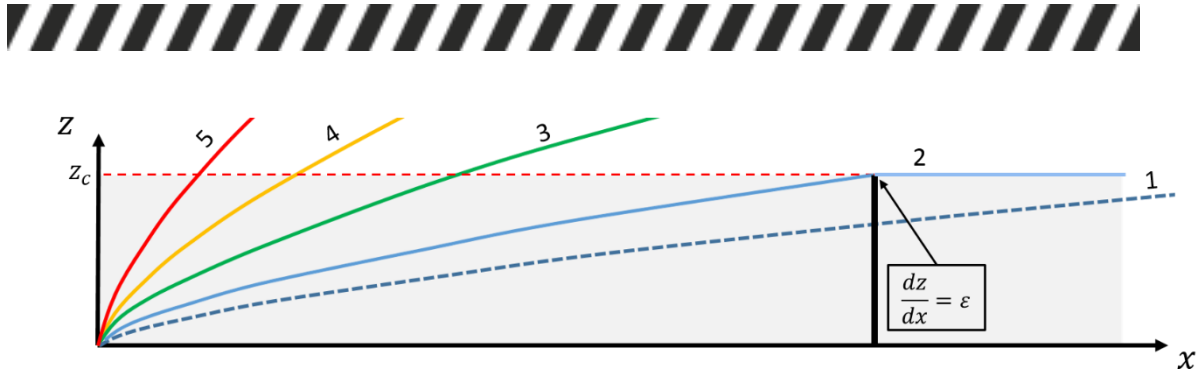


Figure 2: Hypothetical Briggs plume centre-line profiles for different values of the square-bracketed term in Eq. 19. Large-eddy model simulations (Fig. 4) show a general tendency for the plume centre-line to dip below the Briggs centre-line far down-stream of the source. A minimum plume centre-line gradient (ϵ) can be introduced beyond which the plume is considered to have stopped rising.

NUMERICAL SOLUTIONS

Solving the set of differential equations (Eqs. 1—4) numerically requires fewer approximations and assumptions. Background wind speed that varies with height, and variable static stability can be incorporated. Additionally, the plume can possess horizontal velocity in excess of the background wind, although for highly buoyant plume sources, u is often assumed to be small and can be neglected.

The equations can no longer be solved independently, which means a relationship between the dynamic and internal plumes needs to be established. Weil (1988) suggested the LHS of the vertical momentum flux equation be multiplied by the parameter $(1 + k_v)$ where k_v is typically set to a value of 1 for a circular cross-section. Here k_v is an "added" or "virtual" mass coefficient that represents the mass of the ambient air displaced by the plume.

The parameter is necessary because the forcing term on the RHS of Eq. 3 is the area-integrated buoyancy of the internal plume, which acts on the larger dynamic plume (LHS of Eq. 3). Thus, $1 + k_v$ represents the ratio of the dynamic to internal plume cross-sectional areas. Using Briggs' entrainment parameters, the ratio reduces to $(\beta/\beta')^2 = 2.25$, which is a little larger than Weil's suggested value of 2.

In the earliest documented numerical solution to the plume flux equations we could find, Hoult et al. (1969) divided the entrainment velocity, U_n (Eq. 12) into two components to address the significant difference in entrainment rates between vertical and horizontal plumes. They used α for the component of plume flow parallel to the plume axis, and β for the perpendicular component, and assumed the two were additive. In a slightly different approach to the Weil equations, outlined above, they posed the two momentum flux equations (Eqs 2 and 3) with respect to momentum parallel and perpendicular to the plume axis (instead of horizontal and vertical).

Observations of elliptical rather than circular plume cross-sections prompted a reposing of the equations to represent the elliptical structure (e.g., Zhang and Ghoniem 1993, Tohidi and Kaye 2016). Tohidi and Kaye (2016) rederived the Hoult et al. (1969) equations for an elliptical plume cross-section. While the main purpose of that study was to test alternative entrainment closure relationships,



they provided useful comparisons with Briggs solutions (see below), although they did not provide comparisons with solutions assuming circular plume cross-section geometry.

TOHIDI AND KAYE PLUME EQUATIONS

The Tohidi and Kaye equations differ not only in the plume cross-sectional geometry, but also in the coordinates used. Weil and Briggs used a fixed $x - z$ Cartesian coordinate, whereas Tohidi and Kaye follow Hoult et al. (1969) and use natural coordinates aligned with s , the plume axis direction.

$$\frac{dQ}{ds} = Q \sqrt{\frac{2(1+\lambda^2)}{M\lambda}} \left(\alpha \left| \frac{M}{Q} - U \cos \theta \right| + \beta |U \sin \theta| \right), \quad 20.$$

$$\frac{dM}{ds} - U \cos \theta \frac{dQ}{ds} = \frac{FQ}{M} \sin \theta, \quad 21.$$

$$U \sin \theta \frac{dQ}{ds} + M \frac{d\theta}{ds} = \frac{FQ}{M} \cos \theta, \quad 22.$$

$$\frac{dF}{ds} = -QN^2 \sin \theta. \quad 23.$$

The plume's specific volume, momentum and buoyancy fluxes are respectively,

$$Q = \lambda R^2 U_s, \quad 24.$$

$$M = \lambda R^2 U_s^2 = QU_s, \quad 25.$$

$$F = \lambda R^2 U_s b = Qb. \quad 26.$$

The plume cross-sectional area is $\pi R^2 \lambda$, where λ is the ratio of the major to conjugate radii of the non-circular plume cross-section. (Tohidi and Kaye do not appear to provide the value of λ used.) θ is the centre-line trajectory angle from horizontal. U_s is the plume speed parallel to the plume axis, U is the constant ambient horizontal wind speed, and N^2 is the Brunt-Väisälä frequency.

The downstream distance x and height z are given by,

$$x = \int_0^s \cos \theta ds, \quad 27.$$

$$z = \int_0^s \sin \theta ds. \quad 28.$$

While no vertical gradient in the ambient wind term appears on the RHS of the momentum flux equation (as in the Weil formulation), an ambient wind that varies with height can be incorporated. Section 2 of Tohidi and Kaye describes the method used to solve the set of equations, Eqs 20—23.

IN-PLUME TIME AND SPACE VARYING DISTRIBUTIONS

Fig. 3 illustrates the spatial and time-variability of plume flow. The single realization images (left side) give an indication of the instantaneous structure and how it varies from the mean flow represented by the ensemble-average (right side). The bulges on the upper plume edge are caused by buoyancy generated eddies inside the plume. They scale with the plume radius and arise from the



shear between the rising plume and background wind. Weil notes that the instantaneous concentration of plume quantities is relatively constant across the plume with sharp gradients at the instantaneous plume edge. Whereas the time-mean plume quantities have an approximately Gaussian concentration distribution. This implies that, to a rough estimate, the Gaussian variability relates to the relative frequency of plume element presence in the ensemble plume envelope, rather than higher concentrations in the plume centre (or gyre centres). This distinction may be important for our pyroCb tool and ember transport projects.

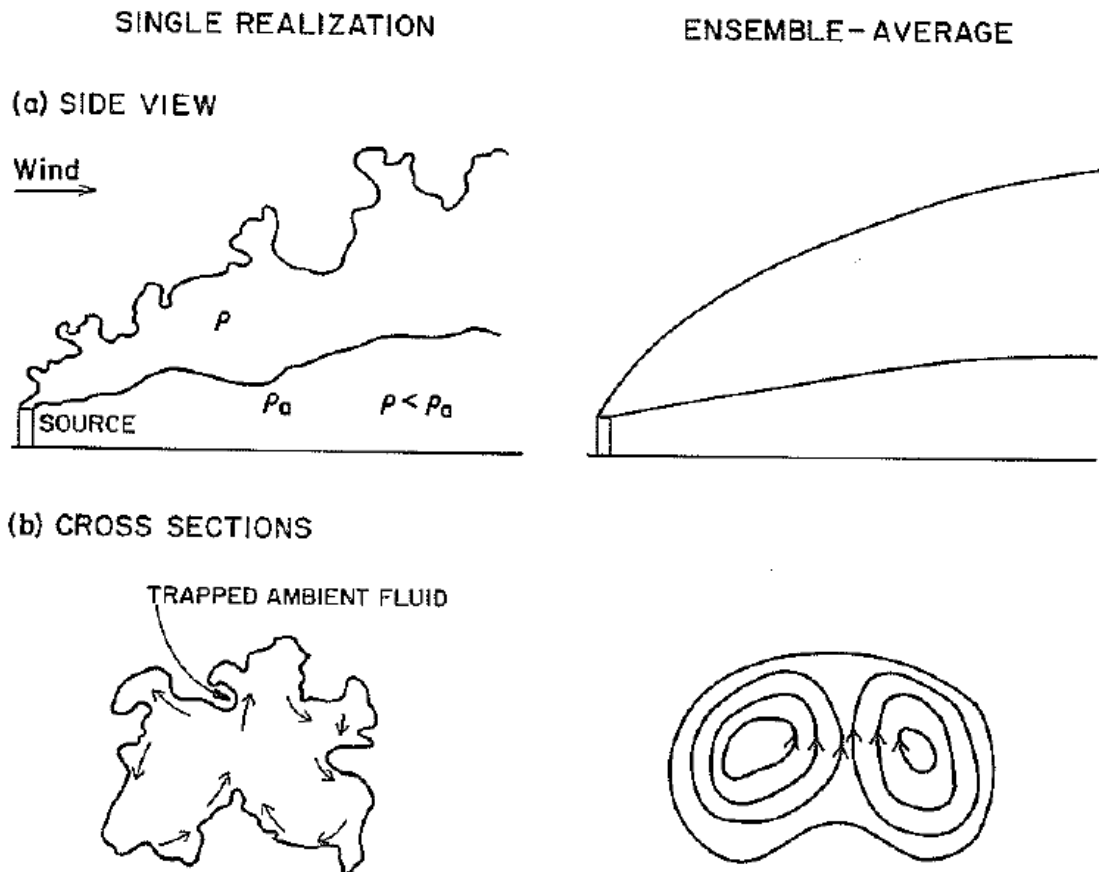


Figure 3: Illustration of instantaneous (left) and time-averaged (right) plume structures, side-on to the background wind (top) and a cross-section perpendicular to the background wind (bottom), reproduced from Fig. 3.1 of Weil (1988).

For the pyroCb tool, a parameter has been included to specify a proportion of the plume cross-sectional area that must exceed a critical height, z_{fc} (see the shaded area in Fig. 1). Choosing a relatively small area would be equivalent to only the turrets on the upper-edge of the plume reaching z_{fc} , whereas choosing half the plume area, or greater, should represent a steady stream of plume elements exceeding z_{fc} .

With respect to the ember transport problem, the top-hat vertical velocity is likely to represent well the instantaneous lofting potential as a function of height, and the Gaussian profile represents the spatial distribution of the frequency of occurrence of this lofting potential.



We have found very few references to studies that have investigated plume quantity distributions. Hübner (2004) showed that the Gaussian distribution represented very well mean plume concentrations for an upright plume (in zero cross-flow) in an environment with ambient turbulence (discussed further below). An elliptical mean plume profile is now widely accepted for plumes in a cross-flow, representing the pair of counter-rotating gyres. If the gyres remain connected a single elliptical Gaussian profile should represent the mean plume concentrations well, but if they separate (see Fig. 3 of Scorer 1959, right panel) a double circular Gaussian might be more appropriate.

The assumed plume profile becomes increasingly important in environments background winds and stability that vary with height, as the vertical scale of the plume grows. In these conditions the top-hat assumption (constant plume quantities across the plume cross-section) becomes questionable as various parts of the cross-section are exposed to different environment conditions. To deal with this problem the plume cross-section may be split into various proportions with different environment interactions. There is a large body of work dedicated to plume penetration into stable environments (e.g., Weil 1988), including improvements to assumed plume geometry.

Double circular connected Gaussian's were also considered for plumes that penetrate a thin inversion (e.g., Weil 1988, Section 3.3.1). The behaviour of the plume is quite sensitive to the proportion of the plume impacted by the inversion. Thus, the double Gaussian geometry was employed to better represent the counter-rotating gyre structure of the bent-over plume, with the expectation that the more realistic plume shape will produce more accurate results.

An additional important consideration of the counter-rotating gyres in the bent-over plume phase is the vertical velocity maximum location in the centre of the plume, which further biases this plume quantity to have larger values at the plume centre.



WILDFIRE APPLICATIONS

HISTORY

Buoyant plume-rise models have only recently been considered for wildfire applications. While we couldn't find any arguments to dismiss such models published in the fire literature, informal discussions with colleagues quoted a few general concerns.

Mature wildfires tend to burn with very large fire fronts, with long near-linear plume sources rather than the much smaller circular chimney sources.

Uncertainty regarding whether solutions valid for elevated chimney stacks should apply to ground-based heat sources.

Uncertainty regarding whether chimney plume results should scale-up to wildfire scales (e.g., wildfire heat sources are orders of magnitude larger, and have orders of magnitude greater buoyancy fluxes).

These concerns are discussed later in this section.

RECENT INTEREST

A few recent studies have identified Briggs-like plume geometry in buoyant plumes generated in laboratory studies (water tanks, wind tunnels, Tohidi and Kaye, 2016) and wildfires (Lareau and Clements 2017).

The wildfire study of Lareau and Clements (2017) fitted the Briggs model to lidar observations to estimate the fire intensity of the El Portal fire in Yosemite National Park, USA, in July 2014. The radius of the observed plume increased linearly with height, and the cross-section of the smoke concentration was found to be Gaussian, both of which agree with plume-rise theory. The intensity was deduced by first estimating the slope of the plume and measuring the background wind speed, from which they were able to determine the net buoyancy flux, and thus fire power. This case study benefitted from conditions on the day of analysis, in which the fire evolved slowly with plume development from "an isolated expanding flank of the fire", as well as a neutrally stratified boundary layer (Lareau and Clements, 2017), whereas in more complex conditions, applicability of the Briggs equations is likely to be relatively constrained.

Our own large-eddy model (LEM) simulations of plumes in a neutral environment with constant background wind, also show Briggs-like plume geometry. Time-mean vertical velocity profiles of LEM plumes are plotted in Fig. 4, for a range of background wind speeds and surface heat fluxes. In each simulation the boundary layer is given time to "spin-up" before the heat flux is applied. This allows a realistic logarithmic wind speed profile to develop (weak winds near the surface increasing to the constant background wind value some distance above). The neutral layer is present only in the lowest 3 km, with a stable layer above. (See Thurston et al. 2017 for more detail.) The Briggs-like plume₂ centre-line geometry is demonstrated in each panel with the addition of a $z \propto x^{\frac{2}{3}}$ line. In each panel the line follows the maximum vertical velocity reasonably closely, although further from the source the plume tends to dip below the line. This is



likely due in part to the plume interacting with the stable layer above, and/or greater down-wind entrainment than the Briggs model assumes. (As the plume reaches the stable layer it loses buoyancy in that warmer environment, which reduces the ascent rate and, in a typical stable layer, rapidly halts the buoyant plume rise.)

An option is being considered for the pyroCb prediction tool to set a minimum plume centre-line gradient (ϵ) beyond which the plume is considered to have stopped rising. This is depicted in Fig. 2. Scenario 2 shows a plume that has just reached this limit at a height z_c , while Scenario 1 will never reach z_c .

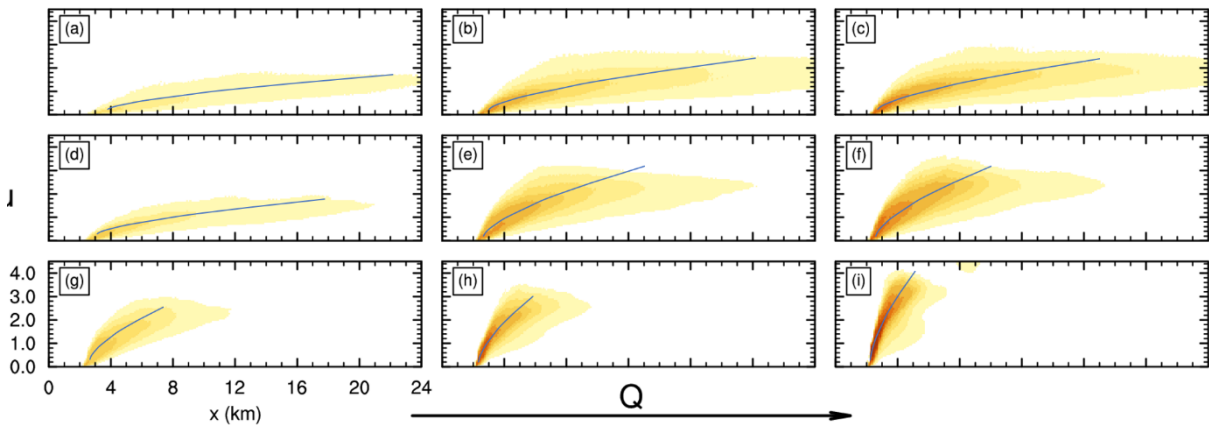


Figure 4: Large-eddy model simulations of the time-mean vertical velocity for a range of buoyancy length scales in a neutral environment below 3 km, and a stable layer above. In each plot a $z \propto x^{\frac{2}{3}}$ line is overlaid to demonstrate the approximate Briggs-like plume centre-line relationship.

As noted above, Tohidi and Kaye (2016) used an advanced integral model that assumes an elliptical plume cross-section geometry, and a double plume entrainment mechanism (i.e., a function of both the along plume velocity difference, and cross-plume velocity difference), with separate entrainment parameters for each component. One of the purposes of that paper is to test various entrainment parameters and two entrainment formulations. A comparison with the Briggs plume-rise model is included as a reference. Each experiment was performed in a neutral atmosphere.

In all cases in which the background flow speed was constant or nearly constant with height, the Briggs model performed very well, often better than the best performing version of the integral model (e.g., Fig. 5). The final set of experiments used data with significant variation in background wind speed near the surface. In these experiments one version of the integral model performed very well, and the Briggs model (which takes a single wind-speed value) over-predicted the plume rise (Fig. 6). Tohidi and Kaye used the surface wind speed rather than a representative wind speed of the overall plume environment, so it is not surprising that this Briggs case performed poorly.

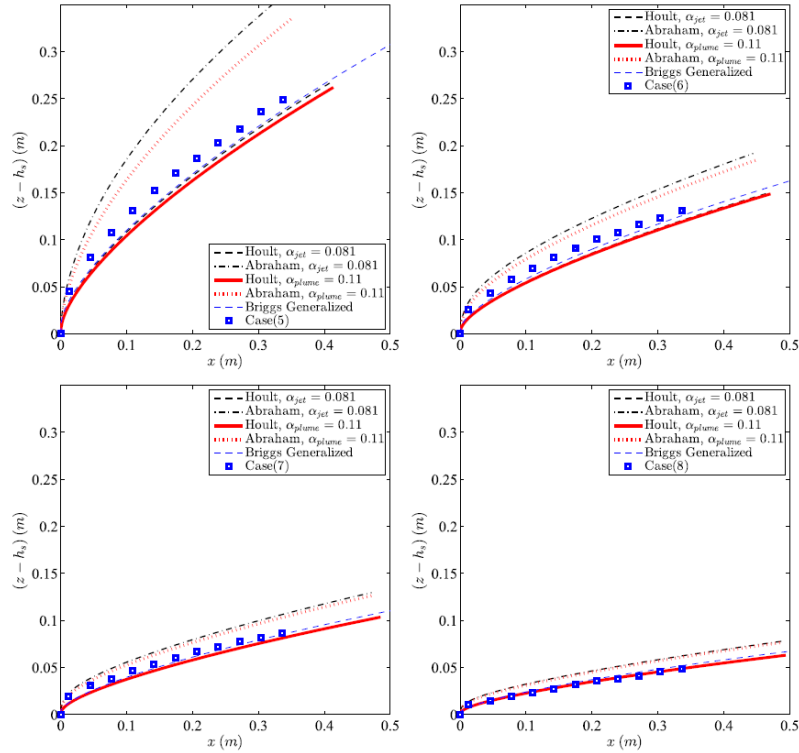


Figure 5: Plots of experimental trajectories (squares) from water tank experiments in neutral stratification (Contini and Robins 2001), compared to two forms of entrainment equations and two entrainment constants (black and red solid and dashed lines) and the Briggs solution (blue dashed line). Cases 5—8 (see last line of the legend) represent essentially an increasing crossflow speed. The figure is reproduced from Fig. 3 of Tohidi and Kaye (2016).

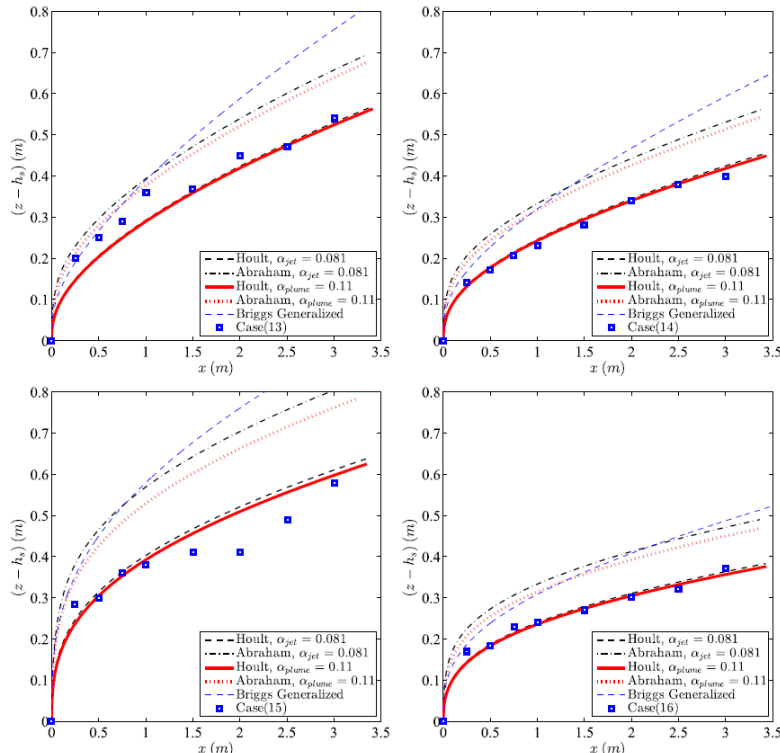


Figure 6: As in Fig. 5 but for atmospheric plume rise observations from elevated sources in an environment with a boundary-layer wind profile (weaker crossflow near the surface). The data is from Marro et al. (2014) and the figure is reproduced from Tohidi and Kaye (2016). Cases 13—16 occur in similar crossflow velocities but decreasing plume buoyancy.



In short, the Briggs plume model performs very well in a neutral atmosphere in which the background wind speed does not vary greatly with height. We expect that if Tohidi and Kaye had chosen a better representative wind speed of the entire mixed layer, the Briggs model would have produced good results. This expectation is based on our experience with the LEM simulations (Fig. 4), with realistic boundary layer wind profiles, that approximate Briggs profiles quite well.

ADDRESSING THE THREE GENERAL CONCERNS

Mature wildfires tend to burn with very large fire fronts, with long near-linear smoke sources rather than circular sources.

Wide-spread fires with multiple flaming zones do tend to produce single broad plumes. Baum and McCaffrey (1989) calculated low-level wind trajectories induced by multiple fires dispersed over many km using a potential flow model and found a central convergence zone developed in all simulations. Even at relatively large heat-source separation distances buoyant plumes can merge and behave like a single larger buoyant plume. This behaviour can be implied from the idealised study of Trelles et al. (1999), although their heat sources were applied to a stable (rather than neutral) environment. Consequently, their plumes rapidly levelled out and began dispersing with minimal buoyancy. They found greater plume rise for sources located parallel to the wind direction, rather than sources located perpendicular to the wind direction. This difference in plume rise is likely due to the relative buoyancy of the plumes at the time of merger, with the former having less combined buoyancy than the latter. We expect plume merger in a neutral atmosphere will also be favoured for downwind heat source separations.

Uncertainty regarding whether solutions valid for elevated chimney stacks should apply to ground-based heat sources.

While the burn-area of most fires is unlikely to be circular, the rising buoyant gases do tend to become organised into an approximately circular cross-sectional area at some elevated level. At this level, there is much in common with buoyant gases emitted from an elevated chimney stack. Kaye and Hunt (2009) showed in a laboratory experiment that plumes developing from a large-area turbulent buoyancy source, contract to approximately half the source diameter to form a circular neck after which the plume expands in a manner similar to a point-source plume. While this study was for a plume in zero background wind, it is likely that the insights gained will also be valid for plumes in a cross-flow, since the neck occurs relatively close to the surface, before any appreciable bend to the plume occurs.

Kaye and Hunt mentioned three papers (Colomer et al. 1999, Friedl et al. 1999, Burelbach 2001) that present experimental results from large-area buoyant sources in which the consensus was that the neck height is approximately equal to one source radius, and the neck is approximately half the source radius. Fig. 7, reproduced from Kaye and Hunt (2009, Fig. 4) illustrates this approximate relationship. The result is very useful for both the pyroCb and ember transport projects, because it provides a good estimate of the height of the fictitious point source of both the Briggs and integral model plumes.

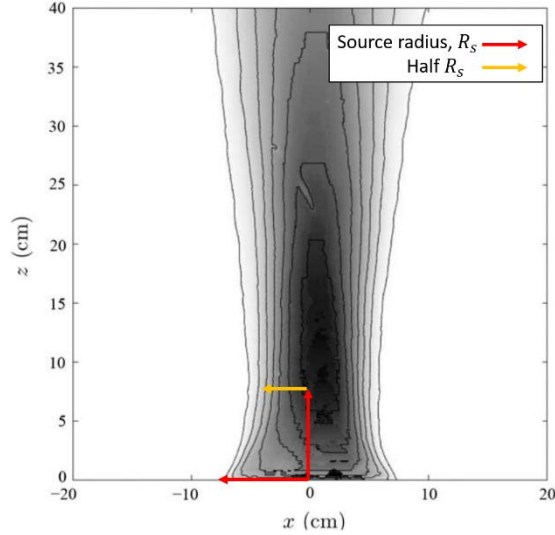


Figure 7: An inverted, unscaled contour plot of a plume with mean buoyancy shaded and contours of constant mean buoyancy. The shading shows $R_{neck} \sim R_s/2$.

If R_s represents the heat source radius (or perhaps the radius of a non-circular heat source expressed as a circle), then the plume radius at the neck $R_{neck} = R_s/2$ and the neck height, $z_{neck} = R_s$. For the upright plume the fictitious virtual source can be determined from the relationship $z = \frac{5}{6\alpha}R$ where $\alpha = 0.08$ is the upright plume entrainment rate. The virtual source height (z_{vs}) below the neck is thus,

$$z_{neck} + z_{vs} = \frac{5}{6\alpha}R_{neck}. \quad 29.$$

Then,

$$z_{vs} = \frac{5}{12\alpha}R_s - R_s = R_s \left(\frac{5}{12\alpha} - 1 \right) = 4.2R_s. \quad 30.$$

However, making the approximation that the bent-over plume has the same geometry from the surface to the neck as the upright plume above, we can apply the same argument to find z_{vs} for a bent-over plume,

$$z_{neck} + z_{vs} = \frac{1}{\beta}R_{neck}. \quad 31.$$

Then,

$$z_{vs} = \frac{1}{2\beta}R_s - R_s = R_s \left(\frac{1}{2\beta} - 1 \right) = -0.17R_s. \quad 32.$$

This corresponds to a virtual source height only a relatively small distance above the surface, which is a fortunate result for the pyroCb and ember transport projects, in which the source radius will be unknown for most applications. For convenience we will assume $z_{vs} = 0$, which means the Briggs solutions can be used without any adjustment for the heat source surface geometry. The schematic presented in Fig. 2 of Scorer (1959), reproduced here in Fig. 8, supports the above conclusion.

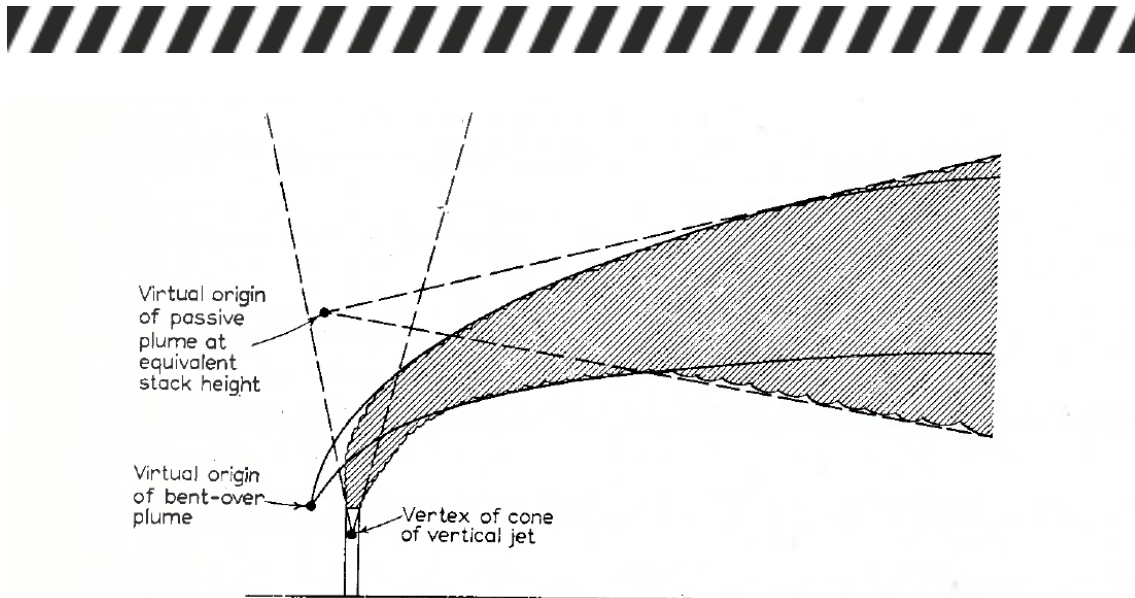


Figure 8: Schematic showing the different heights of various plume-type virtual sources (reproduced from Fig. 2 of Scorer 1959). Note, the virtual source of the bent-over plume is depicted very close to the chimney stack height.

These experiments, like wildfires, meet the "lazy plume" definition: "the near-source flow is dominated by buoyancy-driven acceleration" (Tohidi and Kaye 2016), i.e., the surface buoyancy flux is large compared to the surface momentum flux.

Uncertainty regarding whether chimney plume results should scale-up to wildfire scales (e.g., wildfire heat sources are orders of magnitude larger, and have orders of magnitude greater buoyancy fluxes).

There is no inherent scaling in the plume-rise equations that should exclude larger, more buoyant heat sources (e.g., neglecting viscous effects and Coriolis is valid for wildfires). The vast majority of experiments were performed either in laboratory tanks or the atmosphere above chimney stacks, which already spans scales of several orders of magnitude, with no evidence of scaling limits. Lazy plume conditions were included in some of the experiments documented by Tohidi and Kaye (2016), in which the Briggs model performed well.

Tohidi and Kaye (2016) also suggest that the main distinction between wildfire plumes and industrial waste plumes (from which the Briggs equations were tested and tuned) is orders of magnitude greater buoyancy flux. They propose that as a result, wildfire plumes will have steeper and deeper trajectories near the source and argue that it is important to have a model that can incorporate low-level wind variability, in order to accurately model these plumes (frictional reduction of wind speed is large near the surface). A counter-argument is that the far-field plume shape is dominated by the net buoyancy flux, i.e., it is not greatly influenced by the near-source plume structure, and it is the more remote effects that are more important for our applications. Furthermore, Briggs solutions presented by the Tohidi and Kaye performed well for most cases. The only poor Briggs performance (relative to the integral model) occurred when an inappropriate background wind speed was used (Fig. 6).

One scenario for which the integral model and Briggs equations are likely to be in error is during conditions of high ambient turbulence. Numerous methods to



correct plume centre-line calculations to account for turbulence have been proposed (e.g., Briggs 1975, 1984, Weil 1988). Small-scale turbulence can increase the plume entrainment rate and thus broaden the plume and reduce the plume buoyancy more rapidly. Larger-scale turbulence can carry sections of the plume up and down, producing plume meandering or looping. Turbulence on a sufficiently large scale can break apart a plume exposing it to even greater entrainment. Hübner (2004, PhD thesis, Chapter 6, 7) investigated the response of a laboratory plume with zero background cross-flow to ambient turbulence and found the plume centre-line meandered with the turbulence, while the plume spread was maintained relative to the centre-line, resulting in a much broader time-averaged plume.

For both the pyroCb and ember transport applications, ambient turbulence will act to reduce the potential for sustained pyroCb or ember transport activity but could perhaps increase the potential for short-period bursts when the plumes are embedded in ascending branches of large-scale turbulent flow. Experiments in which surface heat sources were added to our LEM simulations containing boundary-layer rolls revealed significant changes in plume height and vertical velocities depending on whether the heat source was located in an ascending or descending branch of the rolls (see Fig. 9).

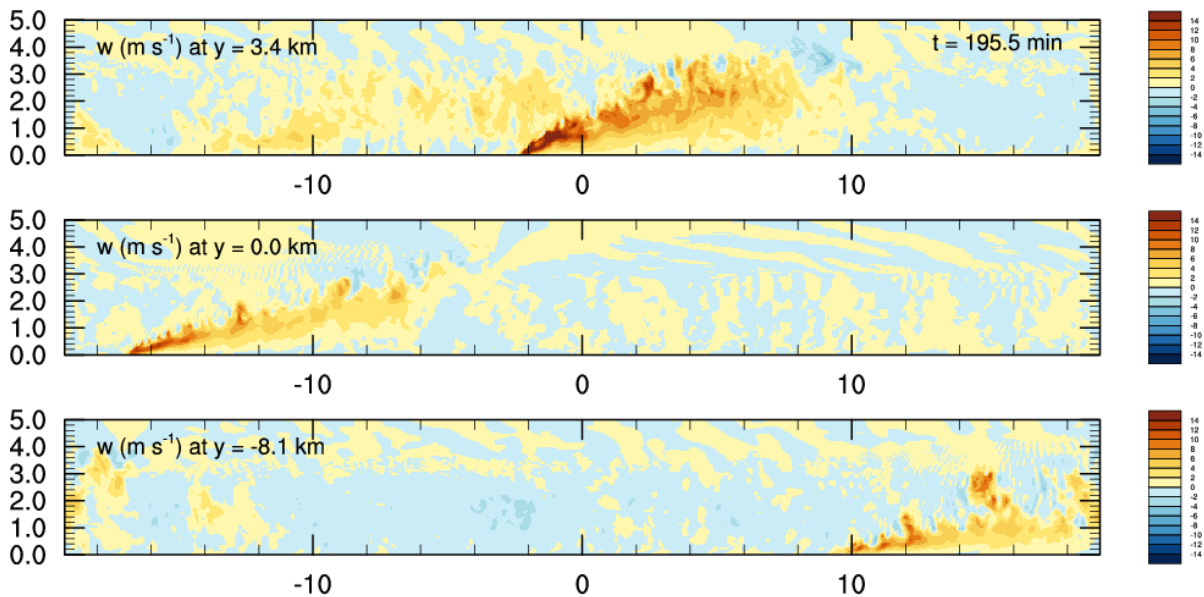


Figure 9: Vertical cross-sections through the plume centres for (upper panel) the plume in the ascending branch of the boundary-layer roll, (middle panel) no boundary-layer rolls, and (lower panel) the plume in the descending branch of the boundary-layer roll. A strong crossflow wind of 15 m s^{-1} was applied in each case with a circular 100 kW m^{-2} , 250 m radius heat source. A surface heat flux of 50 W m^{-2} was used to initiate convective instability in the boundary layer roll cases.



SUMMARY AND DISCUSSION

The study of plume dispersion emerged from the need to design chimney stacks that dispersed pollutants sufficiently to avoid poor air quality for downstream populations. An understanding that the pollutant concentrations generally reduce with the square of the effective stack height, which is a function of the plume centre-line height, led to considerable interest in the prediction of plume-rise trajectories, independent of plume material dispersion. The pyroCb prediction tool and ember transport model projects need to consider both plume rise trajectories and material dispersion.

Solutions to the integral equations assuming top-hat plume quantity distributions have been shown to reproduce plume rise trajectories very well. There are a number of assumptions required to find solutions with associated limitations, but fortunately it would appear the limitations are small for typical wildfire conditions in which pyroCb and ember transport pose a particular threat.

Broad or disparate heat sources tend to produce plumes that initially contract to a circular neck, above which they behave like the classic circular heat source plumes. For bent-over plumes extrapolating the classic Briggs solution below the neck to the surface, produces a virtual source relatively close to the surface. This implies that the Briggs solutions can likely be used without any knowledge of the heat source geometry. The close similarity between the Briggs solutions and the numerical solutions to the full integral equations near the heat source, suggest these solutions can also be applied with no knowledge of the heat source geometry.

The top-hat distribution assumption may become problematic as the plume cross-sectional area becomes large, when different parts of the plume cross-section are exposed to a variable atmospheric environment (e.g., when winds or static stability vary with height). For typical PyroCb conditions a deep well-mixed layer exists with neutral static stability and a near-constant with height background time-mean wind speed, which may or may not be overlaid by a capping inversion. Under the capping inversion the Briggs and numerical solutions should perform very well. A simple approximation suggested by Briggs can be incorporated to ascertain whether or not the plume can penetrate sufficiently to reach the level at which deep buoyant moist convection occurs (and pyroCb can develop). This suggests that the simple analytic Briggs solutions are likely to be sufficient for the pyroCb tool (i.e., there will be no need to find numerical solutions).

We anticipate that the ember transport problem might be more sensitive to background wind speed variability than the pyroCb tool. In the former a good representation of the wind profile will be important for predicting where burning embers will be transported, whereas in the latter we only need to consider plume height and buoyancy. For a more accurate calculation, numerical solutions to the integral model can be used.

This report demonstrates that the Briggs solutions and numerical solutions to the integral equations, should perform very well for the pyroCb and ember transport projects respectively.



REFERENCES

- Arya, S. P., 1999: Air pollution meteorology and dispersion. Oxford University Press, New York, 310 p.
- Baum, H. R. and B. J. McCaffrey, 1989: Fire induced flow-field—Theory and experiment. In: Fire Safety Science: Proceedings of the Second International Symposium. Hemisphere Publishing Newport, Australia, pp 129—148.
- Bennett, M., S. Sutton and D. R. C. Gardiner, 1992: An analysis of LIDAR measurements of buoyant plume rise and dispersion at fiver power stations. *Atmos. Env.*, **26A**, No. 18, 3249—3263.
- Bosenquet, C. H. and J. L. Pearson, 1936: The spread of smoke and gases from chimneys. *Trans. Faraday Soc.*, **32**, 1249—1264.
- Briggs, G. A., 1969: Plume rise. *USAEC Critical Review Series, TID-25075, NTIS*, 81 pp.
- Briggs, G. A., 1975: Plume rise predictions. *Lectures on Air Pollution and Environmental Impact Analyses*, D. A. Haugen, Ed., Amer. Meteor. Soc., 59—111.
- Briggs, G. A., 1984: Plume rise and buoyancy effects. *Atmospheric Science and Power Production*, D. Randerson, Ed., U.S. Dept. of Energy DOE/TIC-27601, available from NTIS as DE84005177, 327—366.
- Byun, D.W., J.K.S. Ching (1999) Science algorithms of the EPA Models-3 community multiscale 755 air quality (CMAQ) modeling system, US EPA, Office of Research and development, EPA/600/R-99/030.
- Carson, J. E. and H. Moses, 1969: The validity of several plume rise formulas. *J. Air Pollt. Control Assoc.*, **19**, 862—866.
- Colomer, J., B. M. Boubnov and H. J. S. Fernando, 1999: Turbulent convection from isolated sources. *Dyn. Atmos. Oceans*, **30**, 125—148.
- Contini, D. and A. Robins, 2001: Water tank measurements of buoyant plume rise and structure in neutral crossflows. *Atmos. Environ.*, **35**, 6105—6115.
- C. Emery, K. Jung, G. Yarwood, 2010: Implementation of an Alternative Plume Rise Methodology in CAMx. Final Report, Work Order No. 582-7-84005-FY10-20.
- De Visscher, A., 2018: Interactive comment on “A Comparison of Plume Rise Algorithms to Stack Plume Measurements in the Athabasca Oil Sands” by Mark Gordon et al. *Atmos. Chem. Phys. Discuss.*
<https://doi.org/10.5194/acp-2017-1093-RC2>.
- Epstein, M. and J. P. Burelbach, 2001: Vertical mixing above a steady circular source of buoyancy. *Int. J. Heat Mass Transf.*, **44** (3), 525—536.
- Friedl, M. J. C. Hartel and T. K. Fannelop, 1999: An experimental study of starting plumes over area sources. *Nuovo Cimento C* 22, 835—845.
- Gordon, M., P. A. Makar, R. M. Staebler, J. Zhang, A. Akingunola, W. Gong and S—M. Li, 2017: A comparison of plume rise algorithms to stack plume measurements in the Athabasca oil sands. *Atmos. Chem. Phys. Discuss.*,
<https://doi.org/10.5194/acp-2017-1093>.
- Holland, J. Z., 1953: A meteorological survey of the Oak Ridge area: Final report covering the period 1948—1952. *U. S. Weather Bureau, USAEC Report ORO-99*, 554—559.
- Holmes, N.S., L. Morawska (2006) A review of dispersion modelling and its application to the dispersion of particles: An overview of different



- dispersion models available. *Atmos. Env.* 40 (30), 5902-5928. doi: 10.1016/j.atmosenv.2006.06.003.
- Hoult, D. P., J. A. Fay, and L. J. Forney, 1969: A theory of plume rise compared with field observations. *J. Air Pollt. Control Assoc.*, **19**, 585—590.
- Hübner, J., 2004: Buoyant plumes in a turbulent environment. Ph. D. Thesis. *University of Cambridge*.
- Im, U., R. Bianconi, E. Solazzo, I. Kioutsioukisa, A. Badiac, A. Balzarini, R. Baróe, R. Bellasio, D. Brunner, C. Chemel, G. Curcuh, H. Denier van der Gon, J. Flemming, R. Forkel, L. Giordano, P. Jiménez-Guerrero, M. Hirtl, A. Hodzic, L. Honzak, O. Jorba, C. Knotem, P.A. Makar, A. Manders-Groot, L. Neal, J.L. Pérez, G. Pirovano, G. Pouliot, R.S. Jose, N. Savage, W. Schroder, R.S. Sokhi, D. Syrakov, A. Torian, P. Tuccella, K. Wang, J. Werhahn, R. Wolke, R. Zabkarn, Y. Zhang, J. Zhang, C. Hogrefe, S. Galmarini (2015) Evaluation of operational online-coupled regional air quality models over Europe and North America in the context of AQMEII phase 2. Part II: Particulate matter, *Atm. Env.*, **115**, 421-441. doi:10.1016/j.atmosenv.2014.08.072
- Kaye, N. B. and G. R. Hunt, 2009: An experimental study of large area source turbulent plumes. *Int. J. Heat Fluid Flow.*, **30**, 1099—1105.
- Lareau, N. P. and C. B. Clements, 2017: The mean and turbulent properties of a wildfire convective plume. *J. Applied Met. and Clim.*, **56**, 2289—2299. doi:10.1175/JAMC-D-16-0348.1.
- Marro, M., P. Salizzoni, F. Cierco, I. Korsakissok, E. Danzi and L. Soulhac, 2014: Plume rise and spread in buoyant releases from elevated sources in the lower atmosphere. *Environ. Fluid Mech.*, **14**, 201—219.
- Morton, B. R., G. I. Taylor, and J. S. Turner, 1956: Turbulent gravitational convection from maintained and instantaneous sources. *Proc. Roy. Soc. London*, **A234**, 1—23.
- Scorer, R. S., 1959: The behaviour of chimney plumes. *Int. J. Air Poll.*, **1**, 198—220.
- Stein, A.F., Draxler, R.R., Rolph, G.D., Stunder, B.J.B., Cohen, M.D., and Ngan, F., (2015). NOAA's HYSPLIT atmospheric transport and dispersion modeling system, *Bull. Amer. Meteor. Soc.*, **96**, 2059-2077, <http://dx.doi.org/10.1175/BAMS-D-14-00110.1>
- Taylor, G. I., 1945: Dynamics of a mass of hot gas rising in the air. *USAEC Report MDDC-919 (LADC-276)*, Los Alamos Scientific Laboratory, NTIS.
- Thurston, W., J. D. Kepert, K. J. Tory and R. J. B. Fawcett, 2017: The contribution of turbulent plume dynamics to long-range spotting. *Int. J. Wildland Fire.*, **26**, 317–330. doi:10.1071/WF16142
- Tohidi, A. and N. B. Kaye, 2016: Highly buoyant bent-over plumes in a boundary layer. *Atmos. Env.*, **131**, 97—114.
- Tory, K. J., W. Thurston and J. D. Kepert, 2018a: Thermodynamics of Pyrocumulus: A Conceptual Study. *Mon. Wea. Rev.*, vol. **146**, No. 8, 2579—2598.
- Tory, K. J., W. Thurston and J. D. Kepert, 2018b: Insights from the development of a pyrocumulonimbus prediction tool. *Research proceedings from the Bushfire and Natural Hazards CRC & AFAC conference, 5—8 September 2018, Perth Australia*.
- Trelles, J., K. B. McGrattan and H. R. Baum, 1999: Smoke dispersion from multiple fire plumes. *American Institute of Aeronautics and Astronautics Journal*, **37 (12)**, 1588—1601.



Weil, J. C., 1988: Plume rise. *Lectures on Air Pollution Modeling*, A. Venkatram, Ed., Amer. Meteor. Soc., 119—166.

Zhang, X. and A. F. Ghoniem, 1993: A computational model for the rise and dispersion of wind-blown, buoyancy driven plumes—1. Neutrally stratified atmosphere. *Atmos. Env.*, **27A**, No. 15, 2295—2311.